Two-Dimensional Simulation of Mass Transfer in Unitized Regenerative Fuel Cells under Operation Mode Switching

Authors:

Lulu Wang, Hang Guo, Fang Ye, Chongfang Ma

Date Submitted: 2018-10-23

Keywords: two-dimensional, transport phenomenon, operation mode switching, regenerative fuel cell, numerical simulation

Abstract:

A two-dimensional, single-phase, isothermal, multicomponent, transient model is built to investigate the transport phenomena in unitized regenerative fuel cells (URFCs) under the condition of switching from the fuel cell (FC) mode to the water electrolysis (WE) mode. The model is coupled with an electrochemical reaction. The proton exchange membrane (PEM) is selected as the solid electrolyte of the URFC. The work is motivated by the need to elucidate the complex mass transfer and electrochemical process under operation mode switching in order to improve the performance of PEM URFC. A set of governing equations, including conservation of mass, momentum, species, and charge, are considered. These equations are solved by the finite element method. The simulation results indicate the distributions of hydrogen, oxygen, water mass fraction, and electrolyte potential response to the transient phenomena via saltation under operation mode switching. The hydrogen mass fraction gradients are smaller than the oxygen mass fraction gradients. The average mass fractions of the reactants (oxygen and hydrogen) and product (water) exhibit evident differences between each layer in the steady state of the FC mode. By contrast, the average mass fractions of the reactant (water) and products (oxygen and hydrogen) exhibit only slight differences between each layer in the steady state of the WE mode. Under either the FC mode or the WE mode, the duration of the transient state is only approximately 0.2 s.

Record Type: Published Article

Submitted To: LAPSE (Living Archive for Process Systems Engineering)

Citation (overall record, always the latest version):	LAPSE:2018.0788
Citation (this specific file, latest version):	LAPSE:2018.0788-1
Citation (this specific file, this version):	LAPSE:2018.0788-1v1

DOI of Published Version: https://doi.org/10.3390/en9010047

energies

MDPI

Article

Two-Dimensional Simulation of Mass Transfer in Unitized Regenerative Fuel Cells under Operation Mode Switching

Lulu Wang [1], Hang Guo [1,2,*], Fang Ye [1] and Chongfang Ma [1]

Received: 16 October 2015; Accepted: 28 December 2015; Published: 15 January 2016
Academic Editor: Peter N. Pintauro

[1] Key Laboratory of Enhanced Heat Transfer and Energy Conservation, Ministry of Education and Beijing Key Laboratory of Heat Transfer and Energy Conversion, College of Environmental and Energy Engineering, Beijing University of Technology, Beijing 100124, China; wanglulusmile@emails.bjut.edu.cn (L.W.); yefang@bjut.edu.cn (F.Y.); machf@bjut.edu.cn (C.M.)
[2] Collaborative Innovation Center of Electric Vehicles in Beijing, Beijing 100081, China
* Correspondence: hangguo@sohu.com; Tel.: +86-10-6739-1612 (ext. 8311)

Abstract: A two-dimensional, single-phase, isothermal, multicomponent, transient model is built to investigate the transport phenomena in unitized regenerative fuel cells (URFCs) under the condition of switching from the fuel cell (FC) mode to the water electrolysis (WE) mode. The model is coupled with an electrochemical reaction. The proton exchange membrane (PEM) is selected as the solid electrolyte of the URFC. The work is motivated by the need to elucidate the complex mass transfer and electrochemical process under operation mode switching in order to improve the performance of PEM URFC. A set of governing equations, including conservation of mass, momentum, species, and charge, are considered. These equations are solved by the finite element method. The simulation results indicate the distributions of hydrogen, oxygen, water mass fraction, and electrolyte potential response to the transient phenomena via saltation under operation mode switching. The hydrogen mass fraction gradients are smaller than the oxygen mass fraction gradients. The average mass fractions of the reactants (oxygen and hydrogen) and product (water) exhibit evident differences between each layer in the steady state of the FC mode. By contrast, the average mass fractions of the reactant (water) and products (oxygen and hydrogen) exhibit only slight differences between each layer in the steady state of the WE mode. Under either the FC mode or the WE mode, the duration of the transient state is only approximately 0.2 s.

Keywords: numerical simulation; regenerative fuel cell; operation mode switching; transport phenomenon; two-dimensional

1. Introduction

URFCs based on PEM electrolyte are reversible electrochemical devices capable of operating in water electrolysis (WE) mode and H_2/O_2 FC mode. In the WE mode, water molecules are split into hydrogen and oxygen with the assistance of external voltage. In the FC mode, hydrogen and oxygen molecules are combined to form water and generate electricity [1–4]. URFCs are used extensively, not only for space or military applications, but also for solar-powered aircraft, satellites, and micro-spacecraft applications [5–7]. Proton exchange membrane (PEM) is a convenient electrolyte technology for both WEs and FCs, as it allows for low operational temperature, quick start, fast response, high power and energy densities [8].

The vast literature on experimental research and modeling of PEMFC deal with the water, heat management (e.g., [9–11]) and mass transport (e.g., [12–14]). Hu *et al*. [13] built a comprehensive

model which accounted for the transport phenomena occurring in the PEMFC such as mass transfer, electrochemical kinetics and charge transport. Singh *et al.* [14] developed a theoretical model to simulate transport phenomena in a PEMFC. The work was dedicated to understanding the transport processes in fuel cells for the purpose of improving heat and water management, and alleviating mass transport limitations. Several articles have been published on experimental research and modeling of PEMWE relating to the hydrogen storage, flow and heat transfer (e.g., [15–18]). Grigoriev *et al.* [18] built a model to identify the important physical and chemical phenomena at high pressure in PEM water electrolysers. The model was also used to optimize the performance of a PEM cell. A large amount of literature on experimental PEM URFC research focuses mainly on the preparation techniques for membrane electrode assembly (MEA), the selection of gas diffusion layer (GDL) materials, and the treatment of corrosion-resistant GDL surfaces in terms of content. In addition, system optimization, the effects of structural and operating parameters on the performance of URFCs have also been experimentally investigated [19–24]. The literature on modeling of PEM URFC is extremely limited and very few articles have been published. Guarnieri *et al.* [8] presented a performance model of a PEM URFC via providing voltage, power, and efficiency under varying load conditions as functions of the controlling physical quantities: temperature, pressure, concentration, and humidification. The model was used as a tool for investigating optimized cell/stack designs and operational conditions. Doddathimmaiah and Andrews [25] constructed a computer model based on Excel and Visual Basic to generate voltage-current curves in both WE and FC modes for PEM URFCs with a range of membrane electrode assembly (MEA) characteristics by modifying the standard Butler-Volmer equation. The effect of key factors such as exchange current densities and charge transfer coefficient on cell performance was analyzed. The two models of PEM URFC mentioned above are both steady state, few models can be found for transient performance investigations.

URFCs play a significant role in the promotion of renewable energy sources (wind or solar energy). In practical applications, URFCs can combine with wind or solar energy to store hydrogen and produce electricity [26]. Therefore, switching between both modes is required to achieve this. URFCs involve several problems in the process of operation mode switching, including material stability, corrosion of carbon-base materials (carbon used as catalyst carrier, gas diffusion layer, and bipolar plate) at the anode during WE mode. These problems result in the reduction of catalyst activity and mass transport limitations. Hence, the performance degrades rapidly [4]. Meanwhile, there are complicated transient interactions between electrochemical reactions and transport processes during the operation mode switching [27]. Jin *et al.* [27] built an isothermal two-dimensional (2D) transient model for regenerative solid oxide fuel cells to investigate complicated multi-physics process during the process of mode switching. Simulation results indicated the trend of internal parameter distributions, such as $H_2/O_2/H_2O$ and ionic, electronic potentials. Similarly, it should be emphasized that an investigation into the fundamental mechanism under operation mode switching can offer important guidance in structure optimization, appropriate selection of operating parameters, and mass transfer enhancement for PEM URFC. However, no accessible literature can be found for this purpose.

This study investigates the transient behavior of URFCs under operation mode switching with a numerical simulation technique. The basic idea of modeling is as follows: (1) a two-dimensional (2D) model is selected because the study aims to observe the transport phenomena along the gas flow channel and the vertical location of the PEM; (2) water is maintained in the gaseous state to simplify the model into single-phase [28,29]; (3) the change in the internal temperature is not considered because the main objective of this study is to investigate the mass and electric transport phenomena; (4) the model involves multicomponent species; (5) operation mode switching is a transient process. (6) the model is coupled with an electrochemical reaction, which involves the electric transport between electrodes and chemicals. On the basis of the basic idea of modeling, a 2D, single-phase, isothermal, multicomponent, transient model is built to investigate the transport phenomena in PEM URFCs when switching from the FC mode to the WE mode. The model is coupled with an electrochemical reaction and considers a set of governing equations, including the conservation of mass, momentum, species,

and charge. This study aims to elucidate the complex mass transfer and electrochemical process under operation mode switching.

2. Model Description

Figure 1 shows the computational domain of a 2D URFC model, which includes a gas flow channel, GDL, catalyst layer (CL) at the hydrogen and oxygen sides respectively, and a PEM sandwiched between the two sides. The gases in the gas flow channel at the hydrogen side are a mixture of H_2 and H_2O, and those in the gas flow channel at the oxygen side are a mixture of O_2 and H_2O.

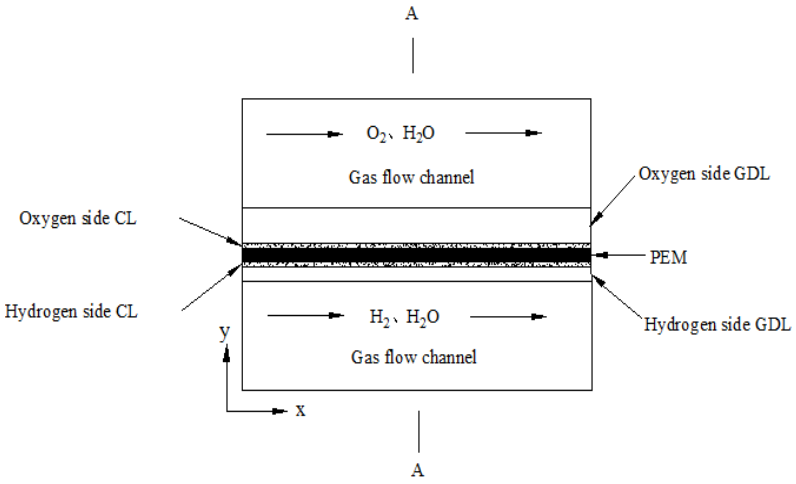

Figure 1. Computational domain of a 2D PEM URFC model.

2.1. Main Hypotheses of the Model

A 2D, single-phase, isothermal, multicomponent, transient model coupled with an electrochemical reaction is built in this study. The model makes the following assumptions:

(1) The temperature inside the URFC is uniform at a constant value of 353 K. Any heat exchange is not considered [14,28].
(2) The Reynolds number and velocity is low. Thus, the flow condition is laminar [13].
(3) GDLs and CLs are isotropic porous media [13,28,29].
(4) The PEM is impermeable to gas species [13].
(5) Water is maintained in the gaseous state [28,29].
(6) Gases are incompressible [14,28,29].

2.2. Governing Equations

2.2.1. Charge Balance

Electrons and ions are transported between oxygen and hydrogen electrode, while PEM only allows ions to migrate through. The charge balance equation based on the generalized Ohm's law can be expressed as follows:

$$\nabla\left(-\sigma_l \nabla \phi_l\right) = \pm a_v i_{\mathrm{loc}} \tag{1}$$

$$\nabla\left(-\sigma_s \nabla \phi_s\right) = \pm a_v i_{\mathrm{loc}} \tag{2}$$

where σ_l and σ_s are ionic and electronic conductivities, respectively. ϕ_l and ϕ_s are ionic and electronic potentials, respectively. a_v is the active specific surface area. The signs in the right side of Equations (1) and (2) are dependent on the cell mode. Table 1 is the selection of signs for equations in FC and WE modes.

i_{loc} in Equations (1) and (2) is the current density that can be described with the Butler-Volmer equation:

$$i_{\mathrm{loc}} = i_0 \left(\exp\left(\frac{\alpha_a F \eta}{RT} \right) - \exp\left(\frac{-\alpha_c F \eta}{RT} \right) \right) \tag{3}$$

where i_0 is the exchange current density, which is dependent on reactant and production concentrations. α_a and α_c are the transfer coefficients for anode and cathode respectively. Overpotential η, is represented by the following equation:

$$\eta = \phi_s - \phi_l - E_{\mathrm{eq}} \tag{4}$$

$$E_{\mathrm{eq}} = E_{\mathrm{eq.ref}} + \mathrm{d}E_{\mathrm{eq}}/\mathrm{d}T \, (T - T_{\mathrm{ref}}) \tag{5}$$

where $E_{\mathrm{eq.ref}}$ is the reference equilibrium potential, E_{eq} is the equilibrium potential, which is a constant in the model because the temperature is constant.

Table 1. Selection of signs for equations in FC and WE modes.

Equations	Mode			
	FC Mode		WE Mode	
	Hydrogen Electrode	Oxygen Electrode	Hydrogen Electrode	Oxygen Electrode
$\nabla(-\sigma_l \nabla \phi_l) = \pm a_v i_{\mathrm{loc}}$	+	-	-	+
$\nabla(-\sigma_s \nabla \phi_s) = \pm a_v i_{\mathrm{loc}}$	-	+	+	-

2.2.2. Multicomponent Mass Transport

The gas transport is described with the Maxwell-Stefan's convection and diffusion equations as follows:

$$\rho \frac{\partial \omega_i}{\partial t} + \nabla \cdot \mathbf{j}_i + \rho (\mathbf{u} \cdot \nabla) \omega_i = R_i \tag{6}$$

$$R_i = \nu_i \frac{a_v i_{\mathrm{loc}}}{n_i F} \tag{7}$$

$$\mathbf{j}_i = -\rho \omega_i \sum_k D_{ik} \mathbf{d}_k \tag{8}$$

$$\mathbf{d}_k = \nabla x_k + (x_k - \omega_k) \frac{\nabla p}{p} \tag{9}$$

$$x_k = \frac{\omega_k}{M_k} M \tag{10}$$

$$\frac{1}{M} = \sum_i \frac{\omega_i}{M_i} \tag{11}$$

Finally, Maxwell-Stefan's equation is:

$$\rho \frac{\partial \omega_i}{\partial t} + \nabla \left(\omega_i \rho \mathbf{u} - \rho \omega_i \sum_{k-1}^{Q} D_{ik} \left(\frac{M}{M_k} \left(\nabla \omega_k + \omega_k \frac{\nabla M}{M} \right) + (x_k - \omega_k) \frac{\nabla p}{p} \right) \right) = R_i \tag{12}$$

where ω_i is the mass fraction of species i, $\mathbf{j}_i$ is the mass flux relative to the mass average velocity, D_{ik} is the multicomponent Fick diffusivity, $\mathbf{d}_k$ is the diffusional driving force acting on species k, x_k is the mole fraction, M is the mean molar mass, and the source term R_i is the rate expression describing its production or consumption.

2.2.3. Gas Flow Equations

Navier—Stokes equations are used to govern the flows in the gas flow channels:

$$\rho\frac{\partial \mathbf{u}}{\partial t}+\rho\left(\mathbf{u}\cdot\nabla\right)\mathbf{u}=\nabla\cdot\left[-p\mathbf{l}+\mu\left(\nabla\mathbf{u}+\left(\nabla\mathbf{u}\right)^{T}\right)-\frac{2}{3}\mu\left(\nabla\mathbf{u}\right)\mathbf{l}\right] \tag{13}$$

$$\frac{\partial \rho}{\partial t}+\nabla\cdot\left(\rho\mathbf{u}\right)=0 \tag{14}$$

Flow in porous electrodes is described with the following Brinkman equations:

$$\frac{\rho}{\varepsilon}\left(\frac{\partial \mathbf{u}}{\partial t}+\left(\mathbf{u}\cdot\nabla\right)\frac{\mathbf{u}}{\varepsilon}\right)=\nabla\cdot\left[-p\mathbf{l}+\frac{\mu}{\varepsilon}\left(\nabla\mathbf{u}+\left(\nabla\mathbf{u}\right)^{T}\right)-\frac{2\mu}{3\varepsilon}\left(\nabla\mathbf{u}\right)\mathbf{l}\right]-\left(\frac{\mu}{\kappa}+\frac{s_m}{\varepsilon^2}\right)\mathbf{u} \tag{15}$$

$$\frac{\partial\left(\varepsilon\rho\right)}{\partial t}+\nabla\cdot\left(\rho\mathbf{u}\right)=s_m \tag{16}$$

where ε and κ, are the porosity and permeability of the gas diffusion layer or catalyst layer, respectively. In addition, the source term s_m is closely associated with the current density:

$$s_m=\sum_i\frac{a_v i_{\mathrm{loc}} M_i}{n_i F} \tag{17}$$

2.3. Initial and Boundary Conditions

The boundary conditions include the average velocity for the inlet of gas flow channel, exit pressure for the outlet of gas flow channel and no slip wall.

The initial conditions:

(1) For the GDL, CL at the H_2 side and PEM: $\phi_l = 0$, $\phi_s = 0$; for the GDL, CL at the O_2 side: $\phi_l = 0$,$\phi_s = \mathbf{V_{cell}}$ (the operating voltage);
(2) The initial values of the oxygen and hydrogen mass fractions are both 0.9.

3. Element Independence Test and Model Validation

3.1. Element Independence Test

The governing equations are solved by the finite element method. The number of elements may have an influence on the results. Therefore, six different number of elements are generated for the model. Figure 2a,b show the oxygen and water mass fractions of a point located at the center of the gas flow channel at the oxygen side changing with the operating voltage under the six number of elements. Figure 2c shows the hydrogen mass fraction of a point located at the center of the gas flow channel at the hydrogen side changing with the operating voltage under the six number of elements. We can observe from Figure 2 that there are no changes in the oxygen, water and hydrogen mass fractions for the number larger than 1410. This observation indicates that the number of elements has no influence on the results. Thus, the number of elements selected is 1410 to reduce the computation time and enhance the accuracy of the results. Figure 3 shows the mesh generation of the model. A structured quadrilateral mesh is created, and the number of the quadrilateral elements is 1410.

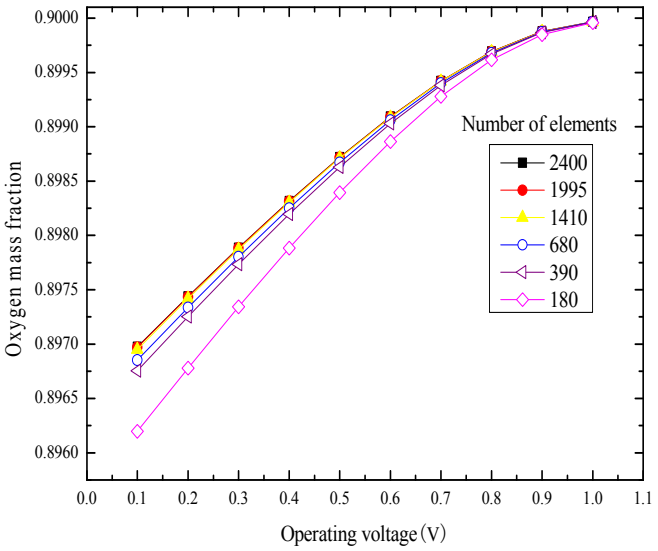

(**a**)

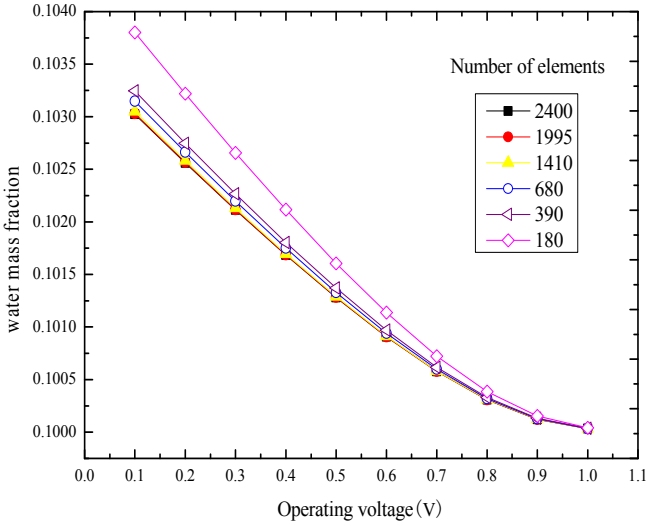

(**b**)

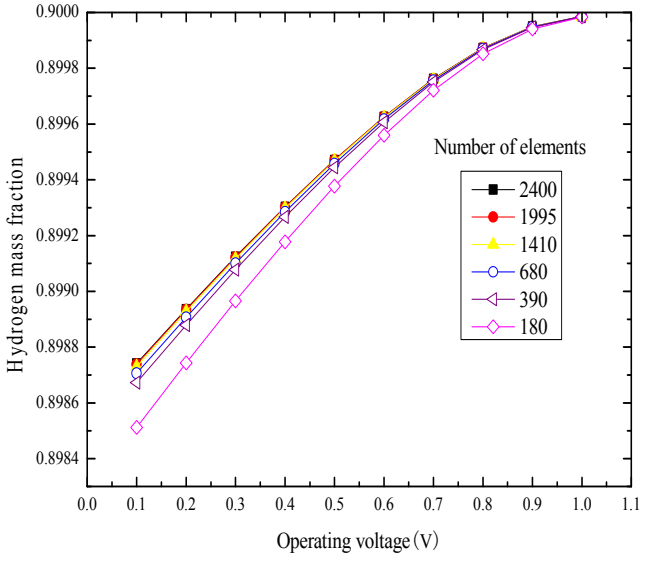

(**c**)

Figure 2. Element independence test for the present mode. (**a**) O_2 mass fraction; (**b**) O_2 side H_2O mass fraction; (**c**) H_2 mass fraction.

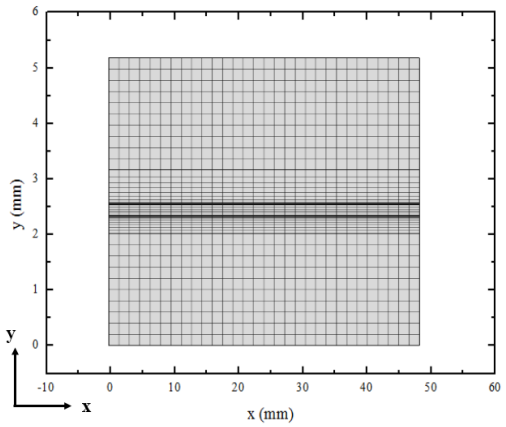

Figure 3. Mesh of the present model.

3.2. Model Validation

The results computed with this model at the steady state are compared with the experimental data in the literature [30], as shown in Figure 4. The numerical model and experimental data are analyzed under the same conditions (ambient temperature and pressure). Notably, the reference transfer current density is adjusted to achieve a good agreement between the present model and the experimental data. Figure 4 shows a slight difference in the I-V curves of the present model and the experimental data. The performance of the present model is better than that indicated by the experimental data in the FC mode. By contrast, the performance indicated by the experimental data is better than that of the present model in the WE mode. Such differences may be explained as follows. On the one hand, the details of the physical parameters used in the experiment are unknown, and the parameters used in the present model do not conform to the experiment fully. On the other hand, the model presents an assumption that water is maintained in the gaseous state. The water generated in the experiment is in the liquid state and may degrade the cell performance by preventing the reactants from reaching the catalyst sites [29,31]. This phenomenon does not occur in the present model. Hence, the results in the experimental data are worse than those obtained with the present model. In the WE mode, water in the liquid state may be distributed more uniformly in the GDL compared with water in the gaseous state. In this case, the experimental data exhibit excellent performance. As such, we can conclude that the present model can be used for related simulations.

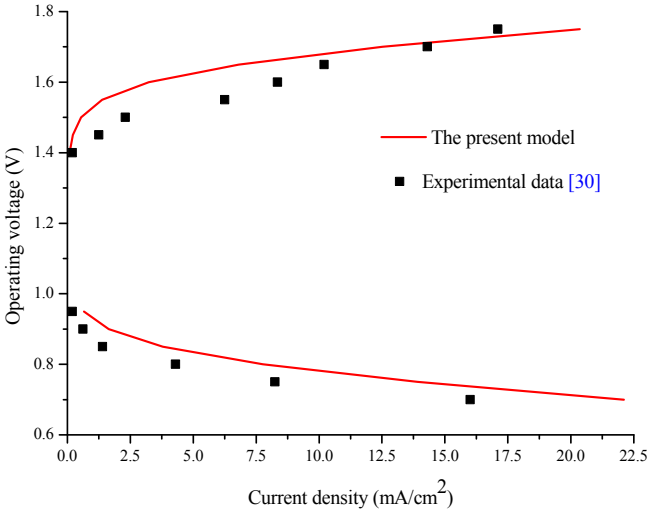

Figure 4. Comparison of the computed URFC performance with the experimental results.

4. Results and Discussion

The transient response of the operating voltage to time under operation mode switching is outlined in Figure 5. The simulation time is set to 5 s. First, the cell functions in the FC mode with an operating voltage of 0.6 V, which is lower than the open circuit voltage (1.23 V). Then, at 0 s, the operating voltage changes from 0.6 V to 1.5 V, which is greater than the open circuit voltage. Correspondingly, the cell switches from the FC mode to the WE mode. Therefore, the minus and plus signs of time symbolize the cell in the FC and WE modes, respectively. The transient transport results under operation mode switching are eventually obtained via numerical simulation. The physical parameters of the URFC and the basic conditions used in this computation are listed in Table 2.

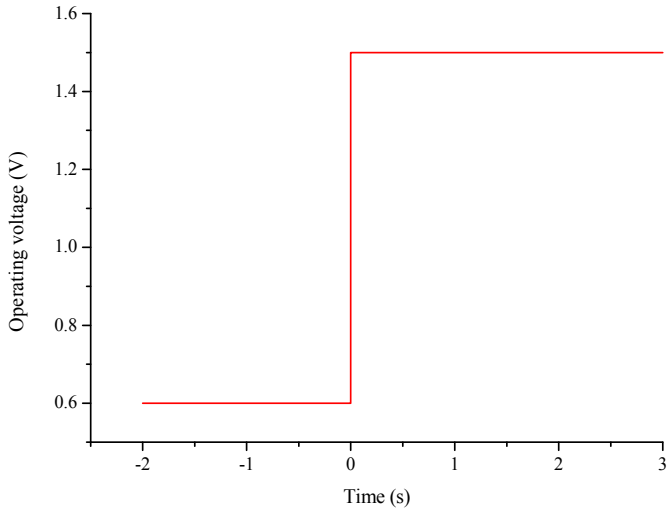

Figure 5. Transient response of the operating voltage to time under mode switching.

Table 2. Physical parameters and basic conditions.

Parameters	Value	References
Length of channel/mm	48	Assumed
Gas flow channel width/mm	2	Assumed
Oxygen electrode GDL thickness/mm	0.6	Assumed
CL thickness/mm	0.028	Assumed
Hydrogen electrode GDL thickness/mm	0.3	Assumed
Membrane thickness/mm	0.178	Assumed
H_2 mass fraction	0.9	[32]
O_2 mass fraction	0.9	[32]
O_2/ H_2 inlet pressure/Pa	1.01×10^5	[32]
O_2 inlet velocity/m·s^{-1}	1.18	[32]
H_2 inlet velocity/m·s^{-1}	0.53	[32]
Oxygen/hydrogen electrode GDL permeability/m^2	1.18×10^{-11}	[32]
Membrane conductivity/S·m^{-1}	1.4	[32]
Oxygen/hydrogen electrode GDL electrical conductivity/S·m^{-1}	1000	[32]
H_2 reference concentration/mol·m^{-3}	56.4	[33]
O_2 reference concentration/mol·m^{-3}	40.8	[33]
Anodic transfer coefficient	0.5	[13]
Cathodic transfer coefficient	0.5	[13]
Operating temperature/K	353	[34]
Hydrogen electrode GDL porosity	0.4	[35]
Oxygen electrode GDL porosity	0.5	[36]
H_2/H_2O binary diffusion coefficient/m^2·s^{-1}	1.22×10^{-4}	Calculated
O_2/H_2O binary diffusion coefficient/m^2·s^{-1}	3.54×10^{-5}	Calculated
Oxygen/hydrogen electrode CL porosity	0.25	Assumed
Active specific surface area/m^{-1}	1.4×10^5	Assumed
Reference temperature/K	298.15	Assumed

Figure 6 shows the hydrogen, oxygen, and water mass fraction distributions along line A–A (as shown in Figure 1, parallel to the *y*-axis at $x = 0.024$ m) at 0 s, which is a special time of the operation mode switching. The cell initially operates in the FC mode. Hydrogen and oxygen are transported from the gas flow channel to the GDL via convection and diffusion. Afterward, hydrogen and oxygen arrive at the CL via diffusion and are consumed at the hydrogen and oxygen electrodes, respectively. Notably, the hydrogen mass fraction decreases from the gas flow channel to the CL along line A–A at the hydrogen side. The oxygen mass fraction exhibits a similar trend in the gas flow channel to the CL along line A–A at the oxygen side. However, compared with the hydrogen and oxygen mass fractions, the water mass fraction at the oxygen side exhibits the opposite trend from the gas flow channel to the CL along line A–A at the oxygen side. This is due to the consumption of H_2, O_2 and the generation of H_2O during the electrochemical reaction.

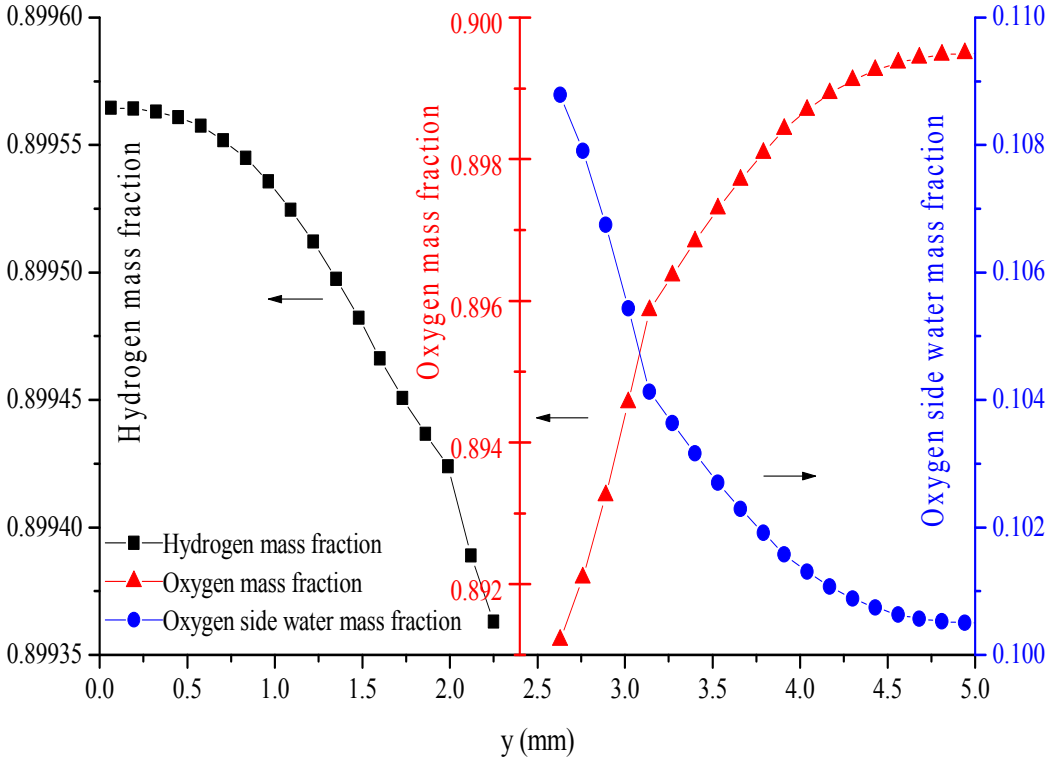

Figure 6. Parameter distribution along line A–A at 0 s.

Figure 7 shows the hydrogen, oxygen, and water mass fraction distributions at the oxygen side along line A–A at 3 s. At 0 s, the operating voltage changes suddenly from 0.6 V to 1.5 V. Thereafter, the switch from the FC mode to the WE mode is achieved. Therefore, the cell functions in the WE mode at 3 s. The water mass fraction at the oxygen side decreases from the gas flow channel to the CL along line A–A at the oxygen side. The minimum of water mass fraction is obtained at the CL. Nevertheless, the oxygen and hydrogen mass fractions exhibit opposite trends from the gas flow channel to the CL along line A–A at the oxygen and hydrogen sides, owing to the generation of O_2 and H_2 during the electrochemical reaction. The maximum mass fractions of oxygen and hydrogen are obtained at the CL.

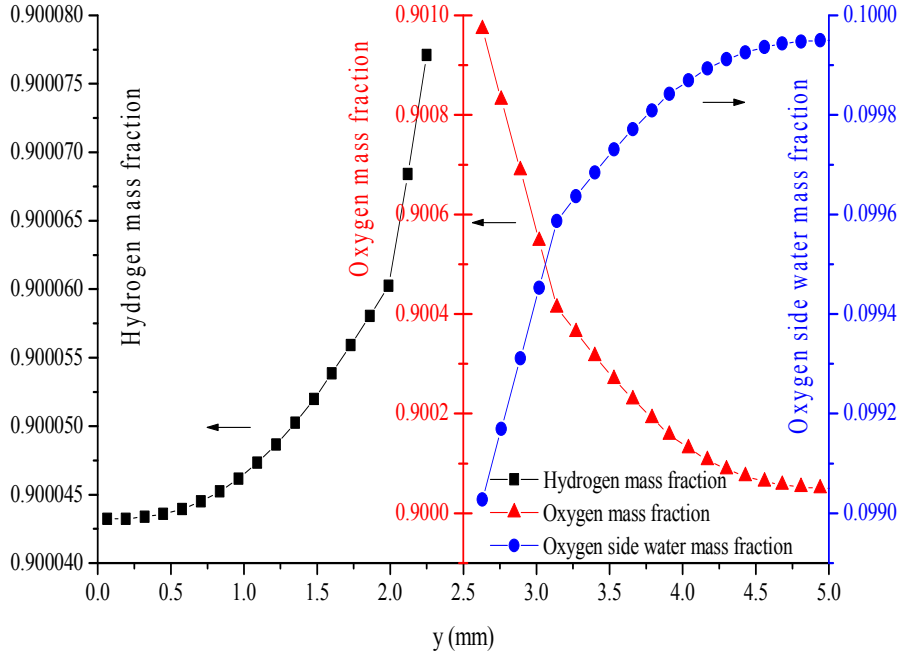

Figure 7. Parameter distributions along line A–A at 3 s.

Figure 8a,b show the time-dependent evolution of the average mass fractions of O_2 and H_2 in different layers. In the first −2 s, the average mass fractions of O_2 and H_2 decrease to the minimum in each layer at approximately 0.2 s and remain unchanged for the rest of time. The electrochemical reaction rate is rapid and only takes a short time to reach the steady state from the transient state in the FC mode. The average mass fractions of O_2 and H_2 exhibit a larger reduction in the CL than in the other two layers because O_2 and H_2 provided in the gas flow channel and supplied to the CL are consumed via the GDL at the oxygen and hydrogen sides, respectively. Differences in the minimum between each layer are evident in the FC mode. At 0 s to 3 s, the average mass fractions of O_2 and H_2 rapidly increase to the maximum from the minimum and maintain constant for the remaining time. The switch from the FC mode toward the WE mode is achieved at 0 s. The duration of the transient state is relatively short that the cell reaches the steady state in approximately 0.2 s. The average mass fractions of O_2 and H_2 exhibit a larger increase in the CL than in the other two layers because O_2 and H_2 are produced in the CL at the oxygen and hydrogen electrodes, respectively. A slight difference in the maximum mass fraction is observed between each layer in the WE mode. We conclude that the average mass fractions of O_2 and H_2 exhibit evident differences between each layer in the steady state of the FC mode and only slight differences between each layer in the steady state of the WE mode. The duration of the switch from the transient state to the steady state in the FC and WE modes is only approximately 0.2 s.

Figure 9 shows the time-dependent evolution of the average mass fractions of O_2 side H_2O in different layers. In the first −2 s, the average mass fractions of O_2 side H_2O increase to the maximum in approximately 0.2 s and maintain constant in different layers. The average mass fractions of O_2 side H_2O increase more significantly in the CL than in the other two layers because water is generated in the CL at the oxygen electrode. The differences in the maximum mass fraction of each layer are significant in the FC mode. At 0 s to 3 s, the average mass fractions of O_2 side H_2O rapidly decrease to the minimum from the maximum and remain unchanged for the rest of time. A significant reduction is observed in the CL compared with that in the other two layers because water is split in the CL at the oxygen electrode in the WE mode. A slight difference is observed in the minimum mass fraction between each layer.

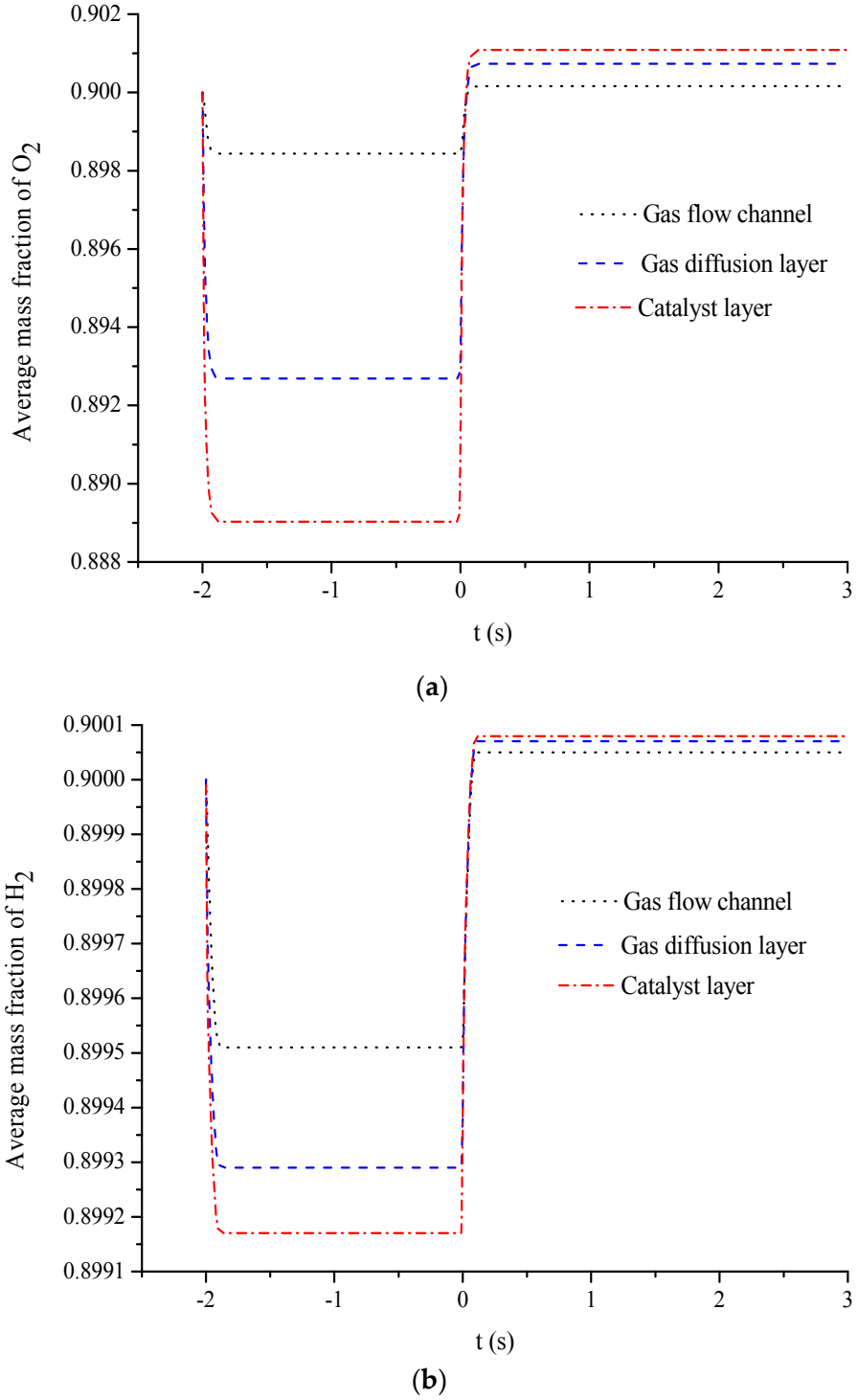

Figure 8. (**a**) Time-dependent evolution of O_2 mass fraction in different layers; (**b**) Time-dependent evolution of H_2 mass fraction in different layers.

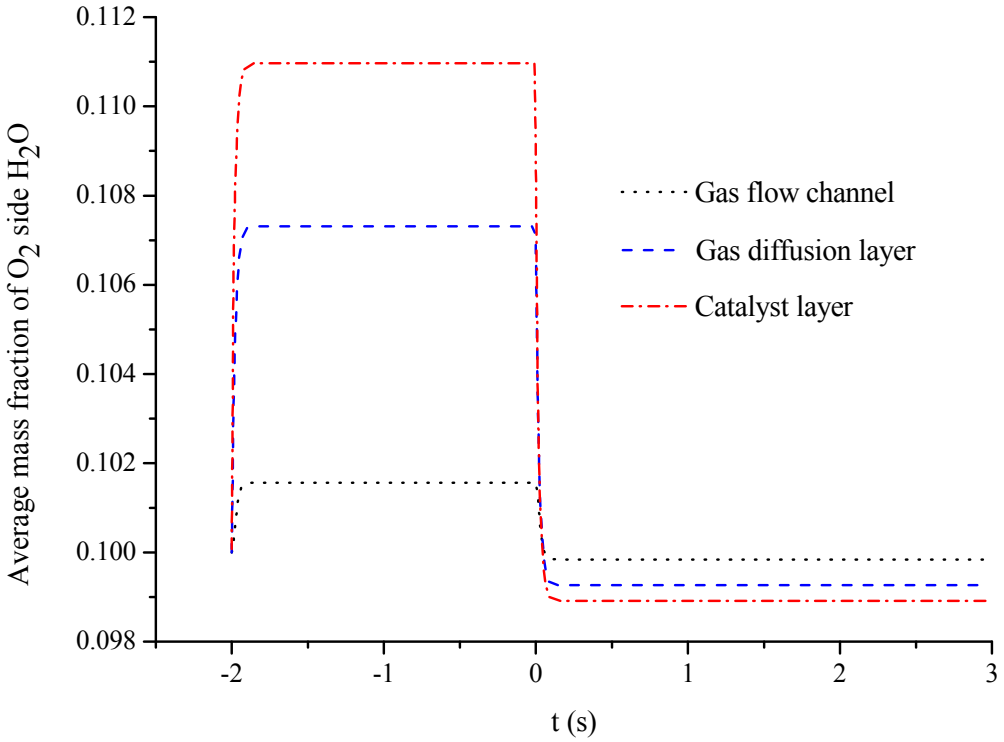

Figure 9. Time-dependent evolution of H_2O mass fraction in different layers.

Figure 10a,b show the 2D distributions of O_2, H_2, and H_2O mass fractions at −0.01 s before the operation mode switching. The cell is in the steady state at −0.01 s according to the Figure 8. Hydrogen mass fraction is distributed uniformly in each layer. On one hand, the electrochemical reaction consumes a little hydrogen, which results in a little reduction in the mass fraction. On the other hand, the excessive hydrogen is provided in the H_2 side gas flow channel, and is rapidly diffused on the surface of CL, a large amount of hydrogen is evenly distributed on the catalyst surface. The oxygen mass fraction decreases with an evident gradient from the gas flow channel to the CL at the oxygen side. However, the water mass fraction exhibits a different trend compared with hydrogen and oxygen; it increases distinctly from the gas flow channel to the CL. Figure 10c,d show the 2D distributions of O_2, H_2, and H_2O mass fractions at 0.01 s after the switching of the FC mode towards the WE mode. The cell is in the transient state at −0.01 s according to the Figure 8. The transient phenomena show that all values of the hydrogen and oxygen mass fractions increase, whereas the overall value of the water mass fraction decreases compared with that at −0.01 s. The hydrogen mass fraction decreases from the inlet of the gas flow channel to the outlet at the hydrogen side and slightly increases near the outlet compared with that at −0.01 s. The oxygen mass fraction also decreases with an evident gradient from the gas flow channel to the CL. Nevertheless, the water mass fraction exhibits the opposite trend along the same direction at the oxygen side. As such, we can conclude that the mass fractions of hydrogen, oxygen, and water respond to the sudden change of operating voltage via saltation under mode switching. The overall electrochemical reaction equation in FC mode is $2H_2 + O_2 \rightarrow 2H_2O$, we can find from this equation that it needs to consume 2 mol (4 g) H_2 and 1 mol (32 g) O_2 to generate 2 mol (36 g) H_2O, the consumption of H_2 mass is smaller than O_2 mass. Therefore, the hydrogen mass fraction gradients are smaller than the oxygen mass fraction gradients for the same scale legend.

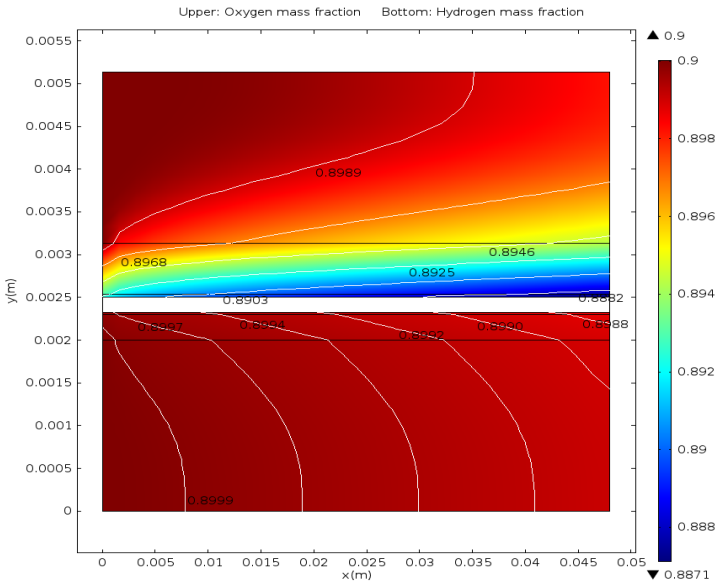

(**a**)

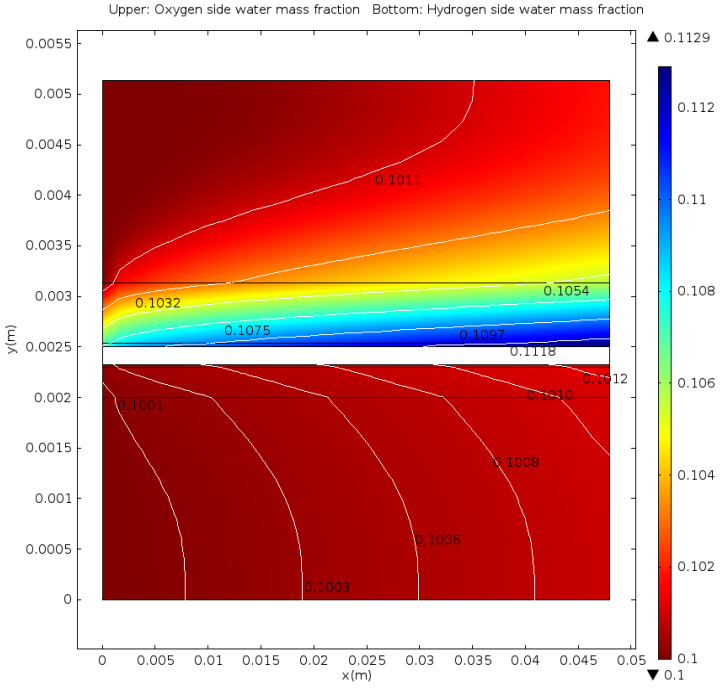

(**b**)

Figure 10. *Cont.*

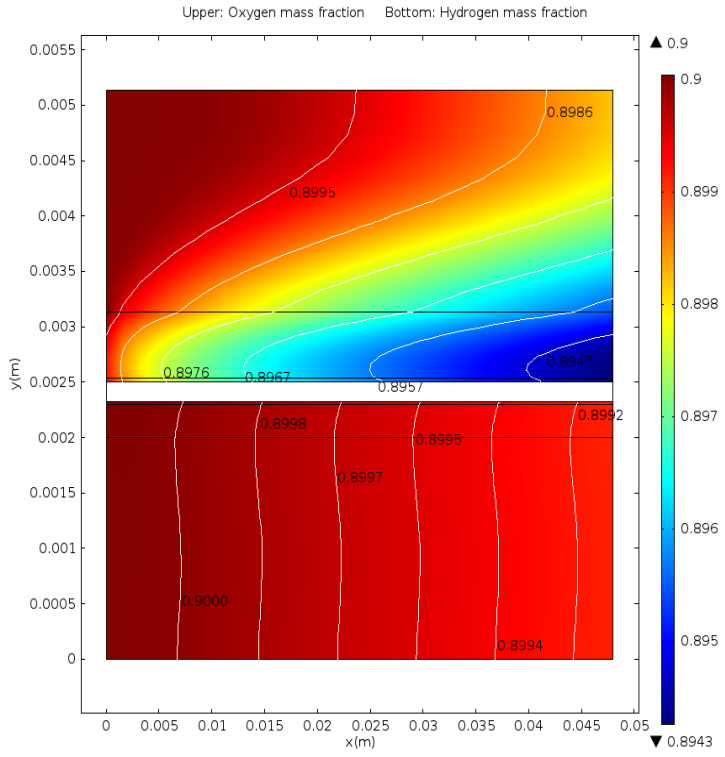

(**c**)

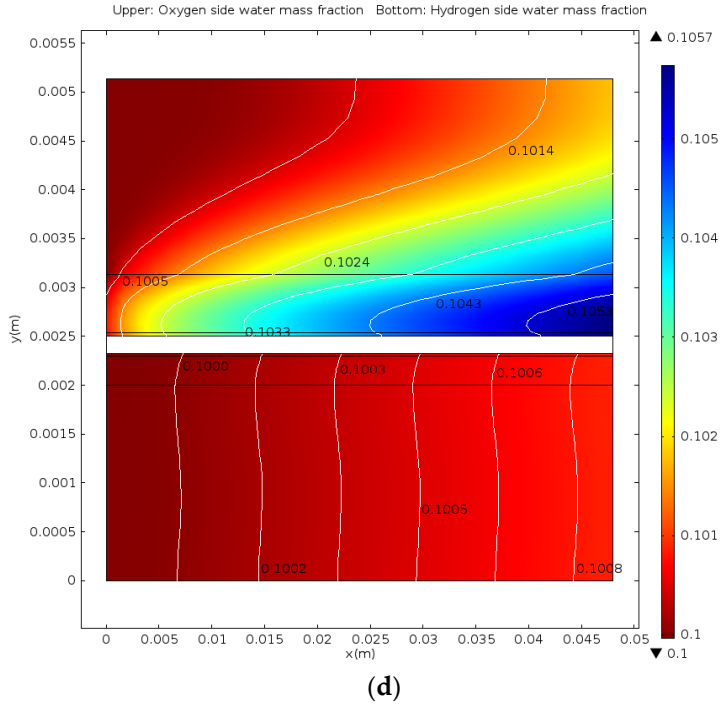

(**d**)

Figure 10. (**a**) Distributions of O_2 and H_2 mass fractions at −0.01 s; (**b**) Distributions of H_2O mass fractions at −0.01 s; (**c**) Distributions of O_2 and H_2 mass fractions at 0.01 s; (**d**) Distributions of H_2O mass fractions at 0.01 s.

The evolution of the electronic potential with time along line A–A under mode switching is shown in Figure 11. The electronic potential is maintained at zero for the hydrogen electrode. However, the electronic potential changes from approximately 0.6 V in the FC mode to 1.5 V in the WE mode at the oxygen electrode during the transient process of mode switching.

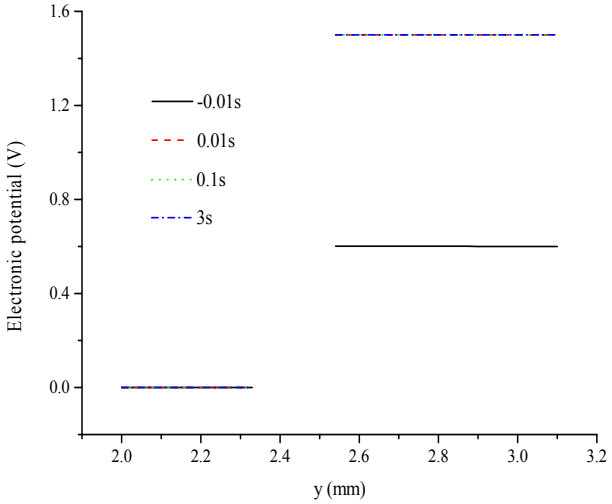

Figure 11. Evolution of electronic potential with time along line A–A in operation mode switching.

Figure 12 shows the evolution of the electrolyte potential with time along line A–A in operation mode switching. At −0.01 and −0.1 s, the cell is in the FC mode. Notably, the electrolyte potential is identical in the FC mode and is approximately −0.2 V at the interface of the CL and membrane of the oxygen electrode. Meanwhile, the electrolyte potential increases linearly from the oxygen electrode to the hydrogen electrode along line A–A and reaches the maximum at approximately 0 V at the hydrogen electrode/membrane interface. At 0 s, the overall value of the electrolyte potential increases considerably. However, the value remains negative. Once the mode is switched from the FC mode to the WE mode, the electrolyte potential changes immediately to the positive value. Then, the electrolyte potential achieves a maximum of approximately 0.15 V at the interface of the CL and membrane of the oxygen electrode by increasing linearly from the hydrogen electrode to the oxygen electrode.

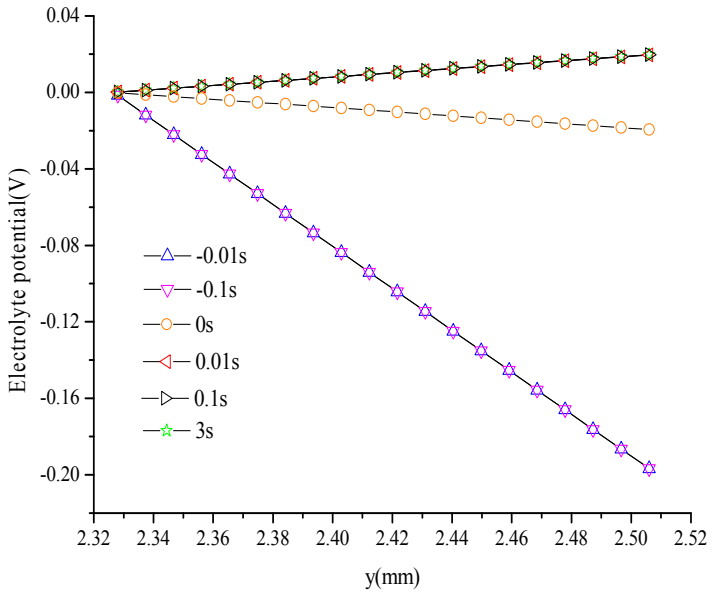

Figure 12. Evolution of electrolyte potential with time along line A–A in operation mode switching.

5. Conclusions

A 2D, single-phase, isothermal, multicomponent, transient model coupled with an electrochemical reaction is built for URFCs, which switch from the FC mode to the WE mode.

(1) The distributions of parameters, such as hydrogen, oxygen, water mass fractions, and electrolyte potential, respond to the operating voltage leap via a sudden change under operation mode switching.

(2) The hydrogen mass fraction gradients are smaller than the oxygen mass fraction gradients for the same scale legend.

(3) Electronic potential exhibits different trends compared with other parameters. At the hydrogen electrode, the electronic potential is maintained at zero in the switching mode. At the oxygen electrode, the electronic potential is maintained at approximately 0.6 V in the FC mode and is switched to approximately 1.5 V in the WE mode. The electrolyte potential increases linearly from the oxygen/hydrogen electrode to the hydrogen/oxygen electrode in the FC/WE mode.

(4) The average mass fractions of the reactants (O_2 and H_2) and product (H_2O) exhibit evident differences between each layer in the steady state of the FC mode. By contrast, the average mass fractions of the reactant (H_2O) and products (O_2 and H_2) exhibit only a slight difference between each layer in the steady state of the WE mode.

(5) The duration of the switch from the transient state to the steady state in either the FC mode or the WE mode is only approximately 0.2 s.

The simulation results presented in this study will help improve our understanding of the internal transport phenomena of URFCs under operation mode switching.

Acknowledgments: The authors are grateful to the National Natural Science Foundation of China (Grant No. 51476003) for the financial support.

Author Contributions: Lulu Wang built the model, organized the data and wrote the main body of the paper. Hang Guo analyzed the numerical results and revised the manuscript. Fang Ye proposed the idea of modeling. Chongfang Ma supervised the research process. All authors read and approved the manuscript.

Conflicts of Interest: The authors declare no conflict of interests.

Nomenclature

	i_{loc}	local current density ($mA \cdot cm^{-2}$)
	i_0	exchange current density ($mA \cdot cm^{-2}$)
	F	Faraday's constant ($C \cdot mol^{-1}$)
	R	gas constant ($J \cdot mol^{-1} \cdot K^{-1}$)
	E_{eq}	equilibrium potential (V)
	$E_{eq.ref}$	reference equilibrium potential (V)
	T	temperature (K)
	T_{ref}	reference temperature (K)
	a_v	specific surface area (m^{-1})
	ω_i	mass fraction of species i
	M_i	molar mass of species i ($kg \cdot mol^{-1}$)
	R_i	reaction source term for species i ($kg \cdot m^{-3} \cdot s$)
	D_{ik}	ik component of the multicomponent Fick diffusivity ($m^2 \cdot s^{-1}$)
	n_i	number of electrons in the reaction
	x_k	molar fraction of species k
	p	pressure (Pa)
	l	entrance length (m)
	j_i	mass flux relative to the mass average velocity ($kg \cdot m^{-2} \cdot s^{-1}$)
	d_k	diffusional driving force acting on species k (m^{-1})
	s_m	mass source term ($kg \cdot m^{-3}$)
Greek letters		
	σ	conductivity of electron of ion ($S \cdot m^{-1}$)
	α	transfer coefficient
	η	over potential (V)
	ϕ	electric potential (V)
	ρ	density of gases ($kg \cdot m^{-3}$)
	ν_i	stoichiometric coefficient
	μ	dynamic viscosity ($Pa \cdot s$)
	ε	porosity of medium
	κ	permeability of medium (m^2)
Subscripts		
	l	ionic
	s	electronic
	a	anodic
	c	cathodic

References

1. Verma, A.; Basu, S. Feasibility study of a simple unitized regenerative fuel cell. *J. Power Sources* **2004**, *135*, 62–65. [CrossRef]
2. Millet, P.; Ngameni, R.; Grigoriev, S.A. Scientific and engineering issues related to PEM technology: Water electrolysers, fuel cells and unitized regenerative systems. *Int. J. Hydrog. Energy* **2011**, *36*, 4156–4163. [CrossRef]
3. Mitlitsky, F.; Myers, B.; Weisberg, A.H. Reversible (unitized) PEM fuel cell devices. *Fuel Cells Bull.* **1999**, *11*, 6–11. [CrossRef]
4. Grigoriev, S.A.; Millet, P.; Porembsky, V.I. Development and preliminary testing of a unitized regenerative fuel cell based on PEM technology. *Int. J. Hydrog. Energy* **2011**, *36*, 4164–4168. [CrossRef]
5. Applyby, A.P. Regenerative fuel cells for space applications. *J. Power Sources* **1988**, *22*, 377–385. [CrossRef]
6. Markgraf, S.; Horenz, M.; Schmiel, T. Alkaline fuel cells running at elevated temperature for regenerative fuel cell system applications in spacecrafts. *J. Power Sources* **2012**, *201*, 236–242. [CrossRef]
7. Yoshitsugu, S. A 100-W class regenerative fuel cell system for lunar and planetary missions. *J. Power Sources* **2011**, *196*, 9076–9080.
8. Guarnieri, M.; Alotto, P.; Moro, F. Modeling the performance of hydrogen-oxygen unitized regenerative proton exchange membrane fuel cells for energy storage. *J. Power Sources* **2015**, *297*, 23–32. [CrossRef]
9. Herrera, O.E.; Wilkinson, D.P.; Merida, W. Anode and cathode overpotentials and temperature profiles in a PEMFC. *J. Power Sources* **2012**, *198*, 132–142. [CrossRef]
10. Zhan, Z.G.; Wang, C.; Fu, W.G. Visualization of water transport in a transparent PEMFC. *Int. J. Hydrog. Energy* **2012**, *37*, 1094–1105. [CrossRef]
11. Nguyen, T.V.; White, R.E. A water and heat management model for proton-exchange-membrane fuel cells. *J. Electrochem. Soc.* **1993**, *140*, 2178–2186. [CrossRef]
12. Ramousse, J.; Deseure, J.; Lottin, O. Modeling of heat, mass and charge transfer in a PEMFC single cell. *J. Power Sources* **2005**, *145*, 416–427. [CrossRef]
13. Hu, G.L.; Fan, J.R. A three-dimensional, multicomponent, two-phase model for a proton exchange membrane fuel cell with straight channels. *Energy Fuels* **2006**, *20*, 738–747. [CrossRef]
14. Singh, D.; Lu, D.M.; Djilali, N. A two-dimensional ananlysis of mass transport in proton exchange membrane fuel cells. *Int. J. Eng. Sci.* **1999**, *37*, 431–452. [CrossRef]
15. Marangio, F.; Santarelli, M.; Cala, M. Theoretical model and experimental analysis of a high pressure PEM water electrolyser for hydrogen production. *Int. J. Hydrog. Energy* **2009**, *34*, 1143–1158. [CrossRef]
16. Nie, J.H.; Chen, Y.T. Numerical modeling of three-dimensional two-phase gas-liquid flow in the flow field plate of a PEM electrolysis. *Int. J. Hydrog. Energy* **2010**, *35*, 3183–3197. [CrossRef]
17. Carmo, M.; Fritz, D.L.; Mergel, J. A comprehensive review on PEM water electrolysis. *Int. J. Hydrog. Energy* **2013**, *38*, 4901–4934. [CrossRef]
18. Grigoriev, S.A.; Kalinnikov, A.A.; Millet, P. Mathematical modeling of high-pressure PEM water electrolysis. *J. Appl. Electrochem.* **2010**, *40*, 921–932. [CrossRef]
19. Jung, H.Y.; Huang, S.Y.; Popov, B.N. High-durability titanium bipolar plate modified by electrochemical deposition of platinum for unitized regenerative fuel cell(URFC). *J. Power Sources* **2010**, *195*, 1950–1956. [CrossRef]
20. Chen, G.B.; Zhang, H.M.; Zhong, H.X. Gas diffusion layer with titanium carbide for a unitized regenerative fuel cell. *Electrochim. Acta* **2010**, *55*, 8801–8807. [CrossRef]
21. Pai, Y.H.; Tseng, C.W. Preparation and characterization of bifunctional graphitized carbon-supported Pt composite electrode for unitized regenerative fuel cell. *J. Power Sources* **2012**, *202*, 28–34. [CrossRef]
22. Huang, S.Y.; Ganesan, P.; Jung, H.Y. Development of supported bifunctional oxygen electrocatalysts and corrosion-resistant gas diffusion layer for unitized regenerative fuel cell applications. *J. Power Sources* **2012**, *198*, 23–29. [CrossRef]
23. Lee, W.H.; Kim, H. Optimization of electrode structure to suppress electrochemical carbon corrosion of gas diffusion layer for unitized regenerative fuel cell. *J. Electrochem. Soc.* **2014**, *161*, 729–733. [CrossRef]
24. Gabbasa, M.; Sopian, K.; Fudholi, A. A review of unitized regenerative fuel cell stack: Material, design and research achievements. *Int. J. Hydrog. Energy* **2014**, *39*, 17765–17778. [CrossRef]

25. Doddathimmaiah, A.; Andrews, J. Theory, modeling and performance measurement of unitized regenerative fuel cells. *Int. J. Hydrog. Energy* **2009**, *34*, 8157–8170. [CrossRef]
26. Hoberecht, M.A.; Robert, D.G. Use of excess solar array power by regenerative fuel cell energy storage systems in low earth orbit. In Proceedings of the IEEE Energy Conversion Engineering Conference, Honolulu, HI, USA, 27 July–1 August 1997.
27. Jin, X.F.; Xue, X.J. Mathematical modeling analysis of regenerative solid oxide fuel cells in switching mode conditions. *J. Power Sources* **2010**, *195*, 6652–6658. [CrossRef]
28. Raj, A.; Shamim, T. Investigation of the effect of multidimensionality in PEM fuel cells. *Energy Convers. Manag.* **2014**, *86*, 443–452. [CrossRef]
29. Ju, H.; Wang, C.Y. Experimental Validation of a PEM fuel cell model by current distribution data. *J. Electrochem. Soc.* **2004**, *151*, A1954–A1960. [CrossRef]
30. Dihrab, S.S.; Razali, A.M. Studies on a single cell unitized regenerative fuel cells. In Proceedings of the 9th ESEAS International Conference on System Science and Simulation In Engineering, Iwate, Japan, 4–6 October 2010.
31. Rabih, S.; Rallieres, O.; Turpin, C.; Astier, S. Experimental Study of a PEM Reversible Fuel Cell, 2011. Available online: http://www.icrepq.com/icrepq-08/268-rabih.pdf (accessed on 17 July 2015).
32. Doubek, G.; Robalinho, E.; Cunha, E.F. Application of CFD techniques in the modeling and simulation of PBI PEMFC. *Fuel Cells* **2011**, *11*, 764–774. [CrossRef]
33. Sehribani, U. Mathematical and Computational Modeling of Polymer Exchange Membrane Fuel Cells. Master's Thesis, University of Nevada, Reno, NV, USA, August 2012.
34. Hsuen, H.K.; Yin, K.M. Performance equations of proton exchange membrane fuel cells with feeds of varying degree of humidification. *Electrochim. Acta* **2012**, *62*, 447–460. [CrossRef]
35. Ni, M. Computational fluid dynamics modeling of a solid oxide electrolyzer cell for hydrogen production. *Int. J. Hydrog. Energy* **2009**, *34*, 7795–7806. [CrossRef]
36. Khazaee, I. Experimental investigation and numerical comparison of the performance of a proton exchange membrane fuel cell at different channel geometry. *Heat Mass Transf.* **2015**, *51*, 1177–1187. [CrossRef]